Sawtooth induced q-profile evolution at ASDEX Upgrade

R. Fischer[1], A. Bock[1], A. Burckhart[1], O.P. Ford[2], L. Giannone[1], V. Igochine[1], M. Weiland[1], M. Willensdorfer[1], and the ASDEX Upgrade Team[1]

[1]Max-Planck-Institut für Plasmaphysik, Boltzmannstr. 2, D-85748 Garching, Germany
[2]Max-Planck-Institut für Plasmaphysik, Wendelsteinstr. 1, D-17491 Greifswald, Germany
Rainer.Fischer@ipp.mpg.de

Abstract. The sawtooth induced q-profile evolution was modelled at ASDEX Upgrade and validated with imaging motional Stark effect (IMSE) measurements. The equilibrium current distribution was estimated by the coupling of a Grad-Shafranov solver and the current diffusion equation. At ASDEX Upgrade an extensive diagnostic suite allows for a reliable modelling of the current density profile and its temporal evolution as long as neo-classical current diffusion can be assumed. The sawtooth-induced central q change, Δq_0, was estimated from equilibrium reconstruction between the sawtooth events without using IMSE measurements. The sawtooth-induced current relaxation is modelled with two different reconnection models, a Kadomtsev full reconnection and a newly developed fully stochastic flat-current model. Both models result in about the same sawtooth-induced $\Delta q_0 \approx 0.10$–0.12 but with a small difference in the absolute q_0 values. The sawtooth-induced evolution of the forward modelled MSE angles agrees well with the IMSE measurements. This confirms the assumption of neo-classical current diffusion between the sawtooth events. A sensitivity study reveals two major ingredients for a reliable interpretation of MSE measurements. Firstly, the sawtooth-induced redistribution of fast ions has to be taken into account for a reliable estimation of the Shafranov shift. The fast-ion redistribution is modelled with a particle-conserving homogeneous fast-ion pressure profile in the plasma core and a subsequent recovery time of 50 ms. Secondly, a reliable estimation of the electric field is necessary for a credible interpretation of the MSE angles.

Keywords: tokamak, equilibrium reconstruction, Grad-Shafranov equation, current diffusion equation, sawtooth instability, full reconnection model, flat-current reconnection model, imaging motional Stark effect, fast-ion redistribution, electric fields, ASDEX Upgrade

Submitted to: *Nucl. Fusion*

I. INTRODUCTION

The current distribution and the corresponding safety factor (q) profile are basic plasma quantities determining the magnetic equilibrium, stability and transport. For advanced operation of fusion devices or even steady-state tokamak operation with high bootstrap current fraction and non-inductive current drive[1,2], a reliable knowledge of the current distribution and the q-profile is necessary. However, a reliable determination of the q-profile in the plasma core with a resolution better than $\Delta q \approx 0.05$ is still a challenging task[3]. A prominent example of this task is given by the ongoing studies to understand the temporal evolution of the q-profile during sawtooth relaxation and the absolute value of the central safety factor, q_0, after the reconnection. Sawteeth were first observed in 1974[4,5]. Measurements of the sawtooth induced q-profile changes were performed at TEXTOR[6], TFTR[7], DIII-D[8], and KSTAR[9,10]. Various reconnection models and various values for q_0 after the sawtooth event have been proposed.

The classical motional Stark effect (MSE) diagnostic, the imaging MSE (IMSE) as an improved variant[11,12], and polarimetry measurements[13] allow internal information about the current distribution to be obtained. Nevertheless, these diagnostics frequently suffer from measurement uncertainties and calibration issues. In particular the absolute calibration of the MSE diagnostic as well as the deterioration by polarised background light is challenging[14,15,16,17,18]. Therefore, the present work proposes an alternative method by calculating the q-profile temporal evolution between sawtooth events and apply different models for the current redistribution of the sawtooth reconnection process. The relative sawtooth induced change, Δq_0, is determined by the evolution and the absolute value slightly depends on the redistribution scheme chosen. This relative change will then be compared to temporal variations of IMSE measurements[11,12].

The present work focuses on q-profile changes due to neo-classical current diffusion combined with two reconnection models, namely the Kadomtsev full-reconnection model and a newly proposed flat-current model (FCM). The equilibrium is reconstructed with a scheme coupling a solver for the Grad-Shafranov equation (GSE) with the neoclassical current diffusion equation (CDE)[19]. Sawtooth effects from fast-ion redistribution, changes in kinetic and rotational profiles and the intrinsic electric fields are considered. It is known that in particular the intrinsic electric field can significantly affect the interpretation of MSE measurements[8,20]. This work shows that the fast-ion redistribution as well as a reliable measurement of the electric field is of major importance. The relative changes of the q-profiles will be validated with IMSE data. The measurements of absolute q-values after the relaxation requires MSE measurements with high absolute precision and will not be subject of this work.

Section II introduces the equilibrium package IDE (Integrated Data analysis Equilibrium) including the GSE, the CDE, and the coupling of both. Section III summarises the Kadomtsev full-reconnection model and introduces the flat-current model. Section IV describes the experiments. Section V shows the importance of the pressure profile, and, in particular, the redistribution of the fast ions for the equilibrium reconstruction. It shows the resulting

sawtooth cycle of the current density and q-profiles, and the q_0 evolution comparing the Kadomtsev model and the FCM. The IMSE measurements are compared with the modelled data and the sensitivity of the MSE angles to the components of the electric field, namely the diamagnetic and rotation terms, and the fast-ion redistribution are shown. Section VI summarises.

II. Equilibrium reconstruction

This section summarises the equilibrium reconstruction at ASDEX Upgrade with the equilibrium package IDE and its recent extensions. A detailed description can be found in [19,21].

The IDE package couples the GSE, describing the ideal magneto-hydrodynamic (MHD) equilibrium for the poloidal flux function ψ in cylindrical coordinates (R, z) for axisymmetric geometry, with the results of the CDE, describing the diffusion of the poloidal flux on the background of the toroidal flux due to resistivity. The GSE

$$\left(R\frac{\partial}{\partial R}\frac{1}{R}\frac{\partial}{\partial R}+\frac{\partial^2}{\partial z^2}\right)\psi = -2\pi\mu_0 R j_\phi(\psi) \quad , \tag{1}$$

with the toroidal current density profile,

$$j_\phi = 2\pi\left(R\frac{\partial p(\psi)}{\partial\psi}+\frac{F(\psi)}{\mu_0 R}\frac{\mathrm{d}F(\psi)}{\mathrm{d}\psi}\right) \quad , \tag{2}$$

depending on the plasma pressure $p(\psi)$ (isotropic case) and $F(\psi)=\mu_0 I_{\mathrm{pol}}/(2\pi)$, with the total poloidal current I_{pol}, describes an equilibrium independent of its history. Typically the solution of the GSE is constrained with external data, e.g. magnetic and scrape-off layer (SOL) current measurements, and internal data, e.g. pressure profiles, polarimetry and MSE measurements, if available. Owing to limited diagnostic capabilities, the equilibrium reconstruction is frequently ill-posed and has to be regularised with *non-physical* spatial smoothness constraints. Nevertheless, the temporal evolution of the current distributions of successive equilibria often shows unreasonable variability not consistent with the current diffusion time. An alternative to ad-hoc temporal smoothness constraints is given by augmenting the set of measurements with the current distribution predicted by the CDE, [22]

$$\sigma_{||}\frac{\partial\psi}{\partial t} = \frac{R_0 J^2}{\mu_0\rho}\frac{\partial}{\partial\rho}\left(\frac{G_2}{J}\frac{\partial\psi}{\partial\rho}\right) - \frac{V'}{2\pi\rho}(j_{\mathrm{bs}}+j_{\mathrm{cd}}) \quad . \tag{3}$$

Details of the calculation of the parallel conductivity $\sigma_{||}$, the auxiliary current drive $j_{\mathrm{cd}} = j_{\mathrm{ec}} + j_{\mathrm{nb}}$ consisting of the electron cyclotron current drive (ECCD) j_{ec} and neutral beam current drive (NBCD) j_{nb}, and the bootstrap current j_{bs}, can be found in [19]. $J = I/(R_0 B_0)$ is the poloidal current function I normalised by the product of the reference radius R_0 and the vacuum magnetic field B_0 at R_0. G_2 is a geometrical quantity and V' is the derivative of the plasma volume V with respect to the effective minor radius ρ [22]. In the previous work the NBCD and the fast-ion density and pressure were taken from TRANSP evaluations which is replaced for the present work with the newly developed RABBIT code [23]. The RABBIT code is included in the IDE package and provides fast-ion profiles in real-time within about 25 ms.

The GSE solver is coupled with the CDE solver successively in time. One time step consists of two parts. First, the CDE Eq. (3) is initialised with an equilibrium given at time t. The CDE is integrated until time $t + \Delta t$, where the next equilibrium is to be calculated. Second, the GSE Eq. (1) is solved at time $t + \Delta t$ with additional constraints from the toroidal current distribution resulting from the CDE. A scheme of the workflow is depicted in[19].

Of major importance for the current estimation and MSE interpretation is a reliable pressure constraint. The pressure consists of the sum of the thermal electron, the thermal ion, and the fast-ion pressure. The electron thermal pressure profile is provided by the integrated data analysis (IDA) suite[24]. The ion thermal pressure is calculated from the ion temperature taken from charge exchange recombination spectroscopy (CXRS)[25] at the heating beam. In case of an ohmic plasma T_i is approximated by a simple fitting function of $T_\mathrm{e}/T_\mathrm{i}$ from Fig. 6d in[26], $T_\mathrm{e}/T_\mathrm{i} = 1 + 0.2/\nu_\mathrm{eff}$, employing the effective collisionality ν_eff[26]. For non-ohmic discharges without CXRS measurements $T_\mathrm{i} = T_\mathrm{e}$ is assumed. For the experiments shown in this work T_i is either estimated using the ohmic formula at the beginning of the discharge or from CXRS data. The ion density is estimated using the electron density subtracted by the fast-ion density and a Z_eff profile[27] assuming as major impurity boron. The density and the scalar pressure of the fast ions are taken from calculations with the RABBIT code[23].

The usual equilibrium reconstruction is performed using magnetic measurements, measurements of the divertor tile currents to allow for constraints of the current in the SOL, pressure constraints, and currents in external poloidal field coils. This data set is routinely available. Polarimetry can be included[13], but the spatial resolution of the two lines-of-sight is poor and the uncertainty is too large to be relevant for sawtooth studies. Some flexibility in the poloidal field coil currents is allowed to compensate for induced vessel currents mainly relevant in the ramp-up and ramp-down phases. The diamagnetic flux measurements[28] are used to assess the loss of fast ions and fast-ion redistribution but is not used for the equilibrium reconstruction due to small but systematic uncertainties.

III. Sawtooth reconnection models

For current redistribution mechanisms other than neo-classical current diffusion, equilibrium reconstruction requires an appropriate time-dependent current relaxation model. Various models for current redistribution due to sawtooth relaxation are available[29,30,31,32,33,34,35]. This work addresses current redistribution based on the Kadomtsev full reconnection model and a flat-current model conserving the $q = 1$ flux surface.

The time points of the sawtooth relaxation events are taken from soft X-ray data[36]. Evaluating the time points from independent measurements instead of internal equilibrium quantities, e.g., from a shear criterion, ensures that the sawtooth events are synchronised with the evolution of all profile measurements.

III.A. Kadomtsev model

The model, proposed by Kadomtsev[29], assumes 2D reconnection. The reconnection evolves simultaneously at a field line on the $q = 1$ surface. The problem is treated using the single-fluid MHD equation in cylindrical geometry. In this regard, Kadomtsev reconnection is identical to the Sweet-Parker formulation[37] of the reconnection due to plasma resistivity at the $q = 1$ surface[38]. Magnetic reconnection of the helical flux starts at the $q = 1$ resonant surface. The flux surfaces with identical value of the helical flux (but opposite direction of the helical fields!) are reconnected defining a strict reconnection rule. Any other type of magnetic field reorganisation or possible solutions are excluded. It leads to the formation of a (1,1) island at the position of the original $q = 1$ surface. During the reconnection of the flux, the (1,1) island grows towards the plasma centre and the O-point of the island becomes the new plasma centre. Thus, the resulting solution has a safety factor value equal to one at the plasma axis, $q_0 = 1$. Everywhere else in the plasma the q-value is larger than one. This process is described in detail in many papers related to the Kadomtsev model[39]. However, this model contradicts experimental measurements of post-cursor modes after the crash, which are often observed[40]. Additionally, the Kadomtsev model is not capable to explain neither the fast crashes in large tokamaks[38] nor the non-linear saturation of the mode amplitude before the crash[41]. The present work focuses on the description of the final state after the crash starting from the initial experimental profiles. Therefore, also the model proposed in the next chapter is not aimed to describe the evolution of the plasma during the sawtooth crash.

III.B. Flat-current model

As pointed out above, the Kadomtsev model is not able to explain the existence of a (1,1) mode at the original position after the sawtooth crash. Therefore, a new model is required for transport codes to describe the sawtooth crash and keep the $q = 1$ surface at the original position after the crash as observed in experiments[40].

During the last decades, several different models were proposed to describe the sawtooth crash: the Kadomtsev model[29], the stochastic model[31,32,33], the quasi-interchange model[34], the Porcelli model[30], and the Kolesnichenko model[35]. The standard approach was to revise the Kadomtsev model of the crash process. Most well known among these models is the Porcelli model[30]. In this model, the reconnection starts as in the Kadomtsev model at the $q = 1$ surface, but it does not go to the final stage and stops at a particular radius inside $q = 1$. This accounts for the observation of partial sawtooth reconnection and can be fitted to experimental results[42]. The drawback of this approach is the existence of an additional free parameter which defines the amount of reconnected flux: the inner radius where the reconnection stops. Both models also suffer from current sheets at the boundaries of the problem. In this work, we try to address the situation differently. We start from the basic physical background of the reconnection process and from the understanding of the limitations of the Kadomtsev model. This model is also motivated by the stochastic hypothesis of the sawtooth relaxation[31,43]. It is well known that the Taylor model describes well the final state of the evolution of a stochastic system like some regimes of the reversed field pinches. These facts were the starting point for

the development of our model.

As discussed above, the Kadomtsev model has a strict rule for the magnetic reconnection. We abandon this rule and allow for all possible reconnection schemes within the $q = 1$ surface. This can be done assuming Taylor relaxation[44] inside the $q = 1$ surface. Such a formulation minimises the plasma energy by modification of the plasma current profile assuming two conditions:

1. Total plasma helicity[45] is conserved: $K_{\mathrm{tot},q=1} \equiv \int_{q\leq 1} \vec{A} \cdot \vec{B}\, dV$, where $\vec{A}$ is the vector potential of the magnetic field $\vec{B}$.
2. The boundary for the relaxation is the $q = 1$ surface. This conserves the position of $q = 1$ representing experimental observations and is in contrast to the Kadomtsev model.

In tokamaks, the Taylor problem has as trivial solution a flat current density inside the problem domain[46]. This gives directly the rule for the crash model implementation in transport codes. The total current within $q = 1$ remains the same after the crash but the plasma current profile becomes flat within the $q = 1$ surface. This flat-current model (FCM) gives complete freedom for the plasma relaxation but it conserves the total helicity and total current within $q = 1$. Additionally, the FCM preserves the position of the $q = 1$ surface after the relaxation process. After the relaxation the current density profile shows a discontinuity at $q = 1$ but no current sheet. The central safety factor remains below unity, $q_0 < 1$. The contour of the flux surfaces is kept constant and will be adapted with the next equilibrium calculation.

In spite of the different formulations, there is a strong connection between the Kadomtsev model and our new model. The Kadomtsev model also conserves the total helicity of the plasma and it can be seen as a Taylor model with the additional constraint for magnetic reconnection[47]. To be explicit, the Kadomtsev constraints are based on (i) a two-dimensional structure of the reconnection, which implies helical symmetry, and based on (ii) the single-fluid approximation for the reconnection process, which assumes the plasma fluid to be attached to the magnetic field lines. An evaluation of the helicity for both models is given below. It should be noted that there are no first-principle arguments that the flux reconnection rule from Kadomtsev is universally valid. Therefore, it can be substituted by other set of rules for plasma relaxation during the sawtooth crash. At the same time, our model without such constraints remains the most *relaxed* variant of the plasma evolution if only the total helicity at $q = 1$ (or slightly outside this surface) is conserved. This does not mean that this model is correct and able to describe the experimental situation. It only means that the model describes the case of complete relaxation with maximal possible stochastisation, which is the limiting case for plasma relaxation. Thus, the implementation of this model gives in some sense the *worst case* scenario. The real situation is likely to be less relaxed compared to our model due to screening effects of the differential plasma rotation and due to the reduced time during which the reconnection is allowed. The main advantage of this model is, that, due to the small shear around the $q = 1$ surface, it allows the presence of a (1,1) mode after the crash at the same place as before, which is seen in the experiment[40].

Fig. 1(a) shows the current density redistribution for the two extreme cases of the Kadomtsev full reconnection model and the fully stochastic FCM for a sawtooth event at

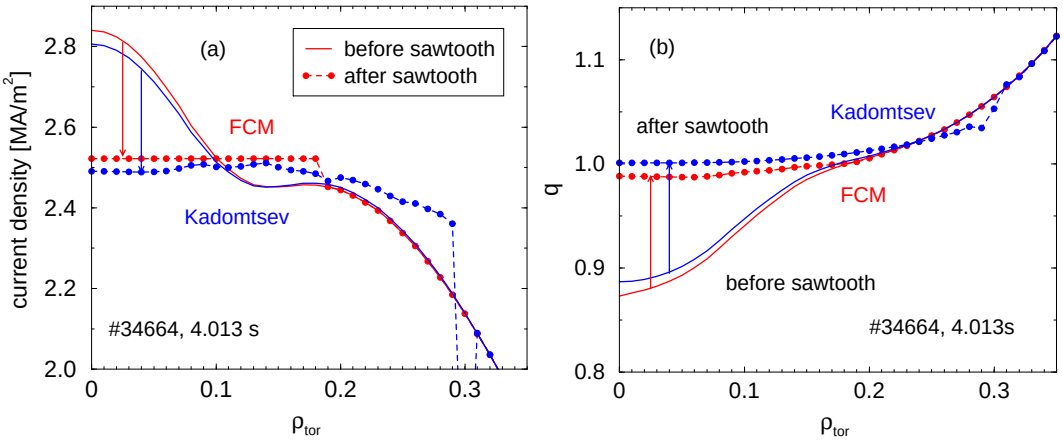

Fig. 1. (a) Current density and (b) q profiles before (solid line) and after (dashed) a sawtooth reconnection event applying the Kadomtsev (blue) and flat-current (red) models.

4.013 s of ASDEX Upgrade discharge #34664. For the Kadomtsev model the relaxed current density at the mixing radius $\rho_{tor} = 0.3$ has the typical discontinuity due to the current sheet. As depicted in Fig. 1(b) this current sheet of the Kadomtsev model results in a large change of the q-profile whereas for the FCM the q-profile is continuous at the mixing radius $\rho_{tor} = 0.2$ given for the FCM by the position of the $q = 1$ surface. The mixing radius is defined as the radius of the outermost surface where the current redistributes. It is given by the reconstructed equilibrium and depends on time and the reconnection model chosen. The redistribution due to the FCM by definition occurs only within the $q = 1$ surface. The q-profile for $\rho_{tor} > 0.2$ ($q \geq 1$) applying the FCM is exactly conserved. Note that the current and q-profiles before the sawtooth event are not the same because all time points before 4.013 s are evaluated with the corresponding relaxation model which results in slightly different equilibria.

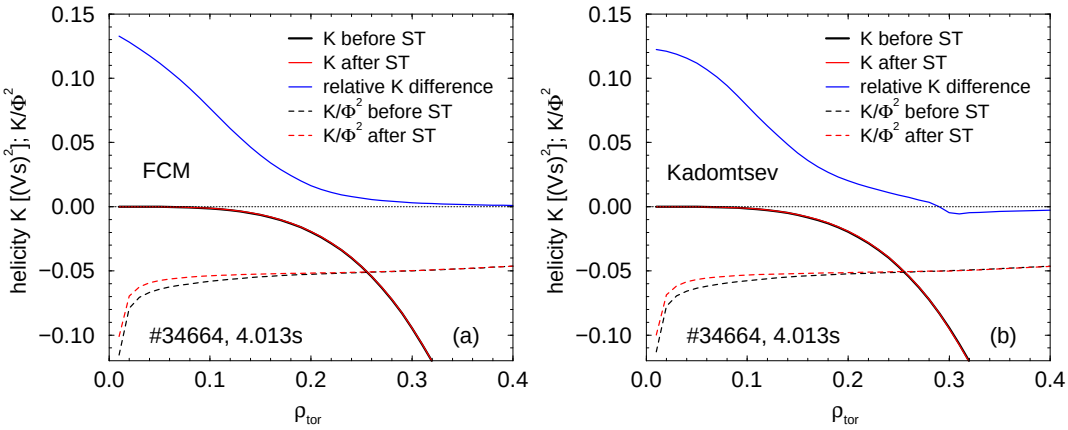

Fig. 2. Plasma helicity (K), plasma helicity normalised to the toroidal flux squared (K/Φ^2), and the relative difference of K before and after the sawtooth reconnection event for (a) the FCM and (b) the Kadomtsev model.

The plasma helicity is evaluated using[45]

$$K = \int_0^{\rho} \frac{2\Phi}{q} d\Phi \tag{4}$$

with the toroidal magnetic flux $\Phi = \pi B_0 \rho^2$ and the effective minor radius ρ[22] ($\rho_{\mathrm{tor}} = \rho/\rho_{\mathrm{boundary}}$). Equation (4) is equivalent to the helicity evaluated using equation (2) in[48]. Note that for uniform q, $K = \Phi^2/q$. Fig. 2 shows the profiles of the plasma helicity (K), plasma helicity normalised with the square of the toroidal flux (K/Φ^2) to emphasise the small difference in the helicity, and the relative difference of K before and after the sawtooth reconnection event for (a) the FCM and (b) the Kadomtsev model. At the mixing radius of the FCM, $\rho_{\mathrm{tor}} = 0.2$ (see Fig. 1(a)), the helicity before and after the sawtooth event differ only by 1.6 %. For the Kadomtsev model the domain with different helicity before and after the event ranges up to its mixing radius of $\rho_{\mathrm{tor}} = 0.3$. The current sheet of the Kadomtsev model can clearly be seen in the helicity difference at about the mixing radius whereas for the FCM the helicity difference is smooth. For both models the helicity is nearly conserved slightly outside of the mixing radius.

IV. Experiments

ASDEX Upgrade discharge #34664 ($I_{\mathrm{p}} = 1$ MA, $B_{\mathrm{t}} = -2.5$ T) shows a rather long phase of similar sawtooth events in a flat-top phase within 2.5–5.0 s with a frequency of about 10 Hz, which can be seen, e.g., in Fig. 7 and Fig 10. Only one neutral heating beam (2.5 MW starting at 2.5 s), suitable for IMSE measurements, and no electron cyclotron resonance heating (ECRH) was used. The core electron density is about $n_{\mathrm{e}} = 4.5 \cdot 10^{19} \mathrm{m}^{-3}$. Fig.

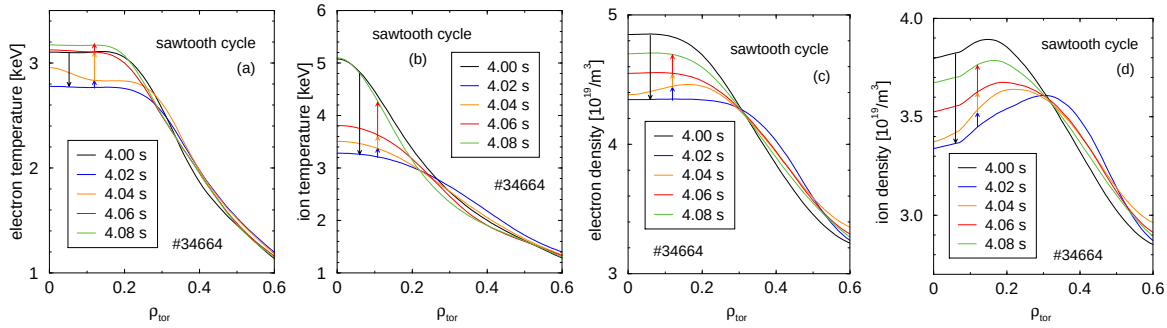

Fig. 3. Sawtooth cycle of (a) electron and (b) ion temperature and (c) electron and (d) ion density profiles.

3 shows a typical example of the sawtooth cycle of the kinetic profiles T_{e}, T_{i}, n_{e}, and n_{i}. The electron temperature T_{e} and density n_{e} is estimated from electron cyclotron emission (ECE)[49], Thomson scattering (TS)[50], lithium beam (LIB)[51] and interferometry (DCN) data within the IDA framework[24]. The ECE diagnostic provides T_{e}-profiles from the plasma centre to the SOL with a dedicated highly-resolved coverage close to the plasma centre. Reliable measurements of T_{e} in the plasma core are essential for a credible evaluation of the current

profile evolution from the CDE. This is due to the large dependence of the current evolution on the conductivity $\sigma_{||}$. Refining relative re-calibration of a few core channels of the absolutely calibrated ECE measurement was performed assuming a constant temperature profile directly after the sawtooth event within the sawtoothing domain. The ion temperature T_i is estimated from CXRS[25]. The main ion density n_i is estimated by subtracting from n_e the fast-particle density, evaluated with the RABBIT code[23], and the assumption of $Z_{eff} = 1.5$ and a major impurity of boron ($Z_{imp} = 5$). The hollowness of the n_i profile is due to the peaking of the fast-particle density (which is not redistributed for Fig. 3(d)). The toroidal fluid rotation velocity

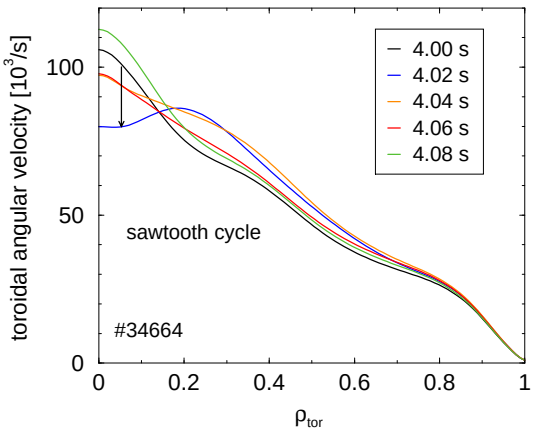

Fig. 4. Sawtooth cycle of toroidal angular velocity of boron

$v_{tor} = \omega_{tor} R$ is estimated from CXRS of boron, where ω_{tor} is the toroidal angular velocity (Fig. 4).

V. RESULTS

This chapter shows the importance of the pressure profile, and, in particular, the redistribution of the fast ions for the equilibrium reconstruction. The sawtooth cycles of the current density and q-profiles are shown and the q_0 evolution applying the Kadomtsev model and the FCM are compared. The reconstructed equilibrium is validated with the measured IMSE data and the sensitivity of the interpretation of the IMSE data on the electric field and the fast-ion redistribution is shown.

V.A. Pressure profiles and fast-ion redistribution

Pressure constraints for the equilibrium reconstruction are evaluated from the measured electron and ion density and temperature profiles and the fast-ion pressure from the neutral heating beam estimated with the RABBIT code[23]. Fig. 5 shows the total pressure data (red circles with uncertainties) used for constraining the equilibrium consisting of the sum of the fast-ion pressure (blue squares) and the thermal electron and ion pressure. The reconstructed equilibrium pressure profile with the corresponding estimation uncertainties

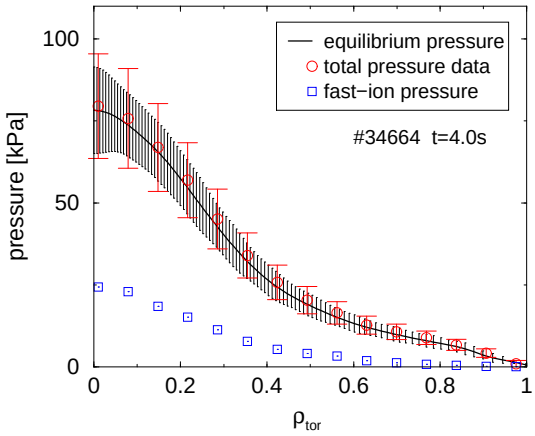

Fig. 5. Reconstructed equilibrium pressure profile (black solid line) and the constraining total pressure data (red circles) where a significant fraction is from the fast-ion pressure (blue squares).

are shown in black. The similarity of the constraining and reconstructed pressure profiles indicates consistency of the pressure profile with magnetic data. Neglecting the fast-ion pressure results in a significant difference between the constraining and reconstructed pressure profiles and a significant difference between the measured and reconstructed diamagnetic flux.

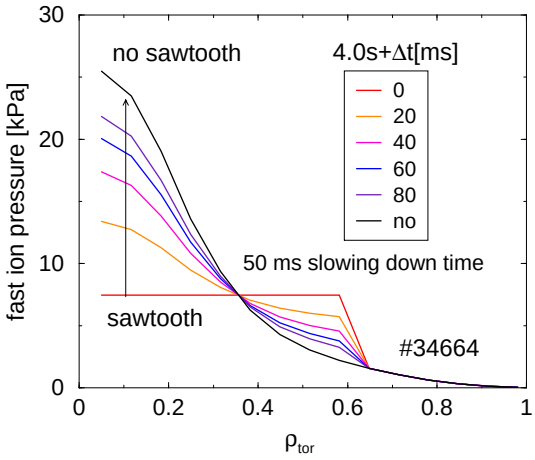

Fig. 6. Fast-ion pressure profiles redistributed after the sawtooth event using particle conservation and a 50 ms recovery time

The magnetic reconnection induced by sawtooth events are known to transport fast ions[52,53]. Fast-ion D-alpha (FIDA) measurements show a significant reduction of the central fast-ion density along with an increase at larger radii. Simultaneously, the loss of fast particles, detected by a fast-ion loss detector (FILD) outside of the plasma[52] and by comparing measured and modelled neutron rates[53], is marginal. The fast-ion density profile reconstructed from the FIDA measurements shows a depletion zone within the inversion

radius and an enrichment up to the mixing radius[53]. The fast-ion density recovers after the sawtooth relaxation with a recovery time of 50–60 ms[52].

Fig. 6 shows a simplified model for the redistribution of fast ions due to sawtooth events which follows closely the experimental observation. Although fast-ion scattering depends on the energy and pitch angle[54], in our simplified model the fast-ion pressure is assumed to be redistributed uniformly. The number of fast particles are assumed to be conserved (no losses). A mixing radius of $\rho_{\mathrm{tor}} = 0.6$ is assumed which resembles the measured value[52,53]. The fast-ion mixing radius is different to the current mixing radii of both, the FCM (0.2) and the Kadomtsev model (0.3). The inversion radius of about $\rho_{\mathrm{tor}} = 0.35$ results from the assumption of particle conservation and the chosen mixing radius. After the sawtooth event an exponential recovery of the calculated fast-ion pressure with a slowing-down time of 50 ms is assumed.

The inversion and mixing radii from ECE measurements for #34664 at $t = 4.013$ s is estimated to be at about 0.32 and 0.73. These values are close to the inversion and mixing radii of the fast-ion redistribution but significantly different from the current redistribution radii. The inversion radius of the T_{e} profile is often used as an indication of the $q = 1$ surface, but it has been demonstrated that they are not necessarily at the same position[55,56]. Generally, for a measured quantity (here T_{e}) significantly less peaked than the current profile, the inversion occurs at larger radii than $\rho_{q=1}$[56].

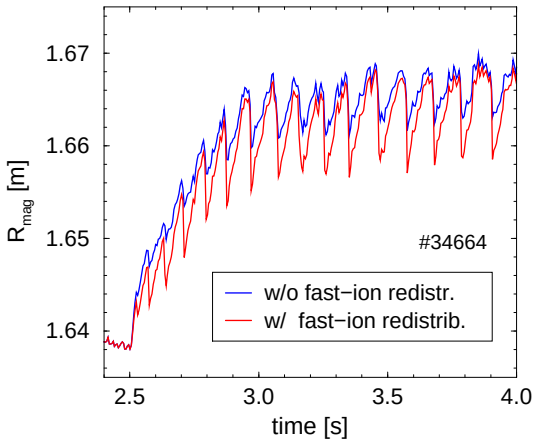

Fig. 7. Temporal evolution of the radial position of the magnetic axis without (blue) and with (red) particle-conserving fast-ion redistribution

The effect of the particle-conserving redistribution of fast ions on the position of the magnetic axis is depicted in Fig. 7. With fast-particle redistribution the sawtooth induced inward shift of R_{mag} is about 10 mm whereas without redistribution considering only relaxation of the thermal profiles it is only about 5 mm. Therefore, for the present case, redistribution of fast particles and relaxation of the thermal pressure contribute similarly to the reduction of the Shafranov shift. After the sawtooth event the pre-sawtooth values of R_{mag} is largely recovered corresponding to the assumed slowing-down time of 50 ms. The uncertainty

of the reconstructed R_{mag}, ΔR_{mag}, is about 6 mm which mainly reflects the uncertainty of 10 % in the pressure profile. Although ΔR_{mag} is in the same order as the difference in R_{mag} with and without fast-particle redistribution, the sawtooth induced redistribution can clearly be seen in the IMSE modelled data (see section V.D).

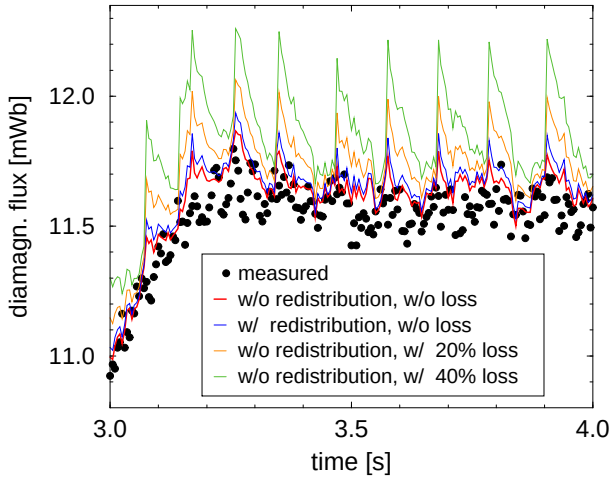

Fig. 8. Measured and modelled diamagnetic flux with no fast-ion redistribution (red), particle conserving redistribution (blue), and no fast-ion redistribution but 20 %/40 % particle loss with a 50 ms recovery time (orange/green)

The FILD measurement does not show any significant loss of fast particles during the sawtooth event[52]. This is confirmed for the present plasma discharge by diamagnetic flux measurements[28]. Fig. 8 compares the measured diamagnetic flux (black dots) with the reconstructed equilibrium diamagnetic flux for different assumptions for the fast-ion redistribution and fast-ion loss. The red line depicts the diamagnetic flux without redistribution and without loss of fast particles. The blue line depicts the diamagnetic flux with particle-conserving fast-ion redistribution as described above which coincides very much with the red line. Both evaluations agree reasonably well with the measured value with only about 0.1 mWb offset which is well below the measurement uncertainty. The situation changes significantly when loss of fast particles is assumed. The orange/green line depicts the diamagnetic flux without redistribution but with a 20 %/40 % loss of fast particles on the entire fast-ion pressure profile, respectively. At each sawtooth the simulated decrease of fast-ion pressure results in a decrease of the MHD energy and a corresponding increase of the diamagnetic flux. A recovery with the same 50 ms slowing down time as for the redistribution scheme is assumed. In contrast to the particle-conserving redistribution, a clear sawtooth signature is predicted which is not observed in the measurement. Therefore, we conclude that a loss of fast particles is well below 20 % also for this plasma discharge.

V.B. Sawtooth cycle of current density and q-profiles

Profiles of the flux-surface averaged toroidal current density and the corresponding q-profiles during a sawtooth cycle are shown in Fig. 9. The sawtooth event is at 4.013 s. The FCM was

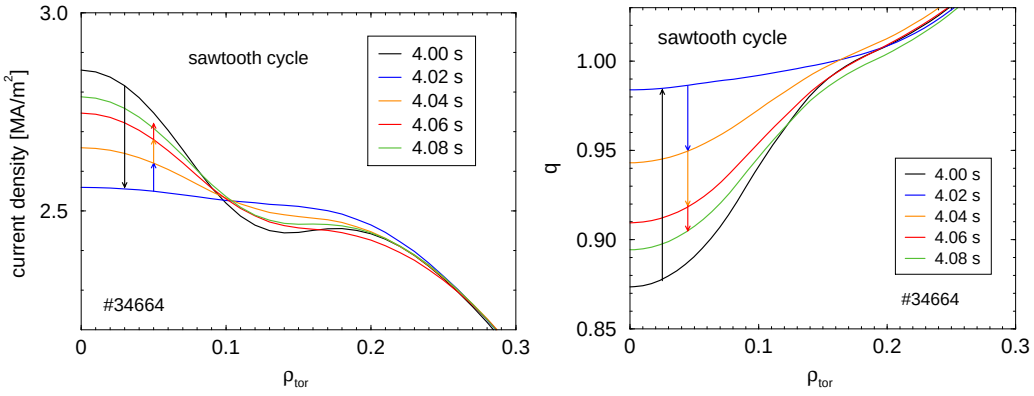

Fig. 9. Profiles of the flux-surface averaged toroidal current and the corresponding q-profiles during a sawtooth cycle.

applied which results in a central q-value after the sawtooth event (blue line) $q_0 < 1$. After the sawtooth the current profile peaks corresponding to a decreasing q_0 evolution. The highly shaped current profile with a significant dip in the interval $\rho_{\mathrm{tor}} = 0.1 - 0.2$ results from the current diffusion only. Equation (3) shows that the current diffusion increases with decreasing radius ρ.

V.C. q_0 evolution

The evolution of the q_0-value is depicted in Fig. 10. The left panel shows q_0 for the complete

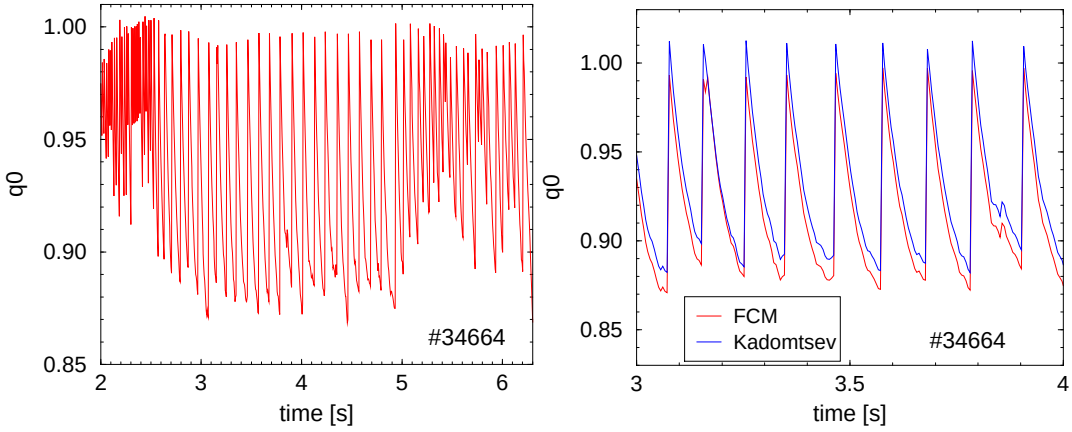

Fig. 10. Temporal evolution of q_0 and a comparison between the Kadomtsev model (blue) and the FCM (red).

flat-top phase employing the FCM. The right panel shows in the time interval 3–4 s q_0

comparing the FCM (red) with the Kadomtsev model (blue). The q_0 values are calculated at the equilibrium time points which are not exactly synchronised with the sawtooth time points. Although the basic level applying the two models is slightly different, the temporal behaviour (decay length) as well as the sawtooth induced q_0 change, Δq_0, is nearly the same. Δq_0 ranges within 0.10–0.12. Even though the two models are extreme cases in the sense of a strict reconnection rule versus a fully stochastic reconnection, the difference between the two models is only about 0.01. This seems to be too small to be resolved experimentally. Nevertheless, the newly proposed model allows for a (1,1) sawtooth post-cursor at the same position as the original $q = 1$ surface as seen in the experiment. In contrast, the Kadomtsev model does not allow a post-cursor because the $q > 1$ everywhere in the plasma. The same small difference can be observed in Fig. 1(b) for the q-profile in the sawtooth affected area. This small difference is advantageous as it allows robust equilibrium reconstruction in the presence of sawteeth nearly independent on the relaxation model chosen.

V.D. imaging MSE

The IMSE diagnostic at ASDEX Upgrade provides a sensitive and robust measurement of the current distribution in the plasma centre[11,12]. The MSE diagnostic measures the polarisation angle of Stark broadened neutral beam D_α emission where the electric field in the rest frame of the beam neutrals is the relevant parameter. The IMSE system measures a 2D image of radiation from the neutral beam. It uses a set of birefringent plates and polariser to modulate the image spatially with interference patterns that encode the polarisation state[12]. The MSE angle γ is calculated using

$$\tan(\gamma) = \frac{A_1 B_\mathrm{r} + A_2 B_\mathrm{t} + A_3 B_\mathrm{z} + A_4 \tilde{E}_\mathrm{r} + A_5 \tilde{E}_\mathrm{z}}{A_6 B_\mathrm{r} + A_7 B_\mathrm{t} + A_8 B_\mathrm{z} + A_9 \tilde{E}_\mathrm{r} + A_{10} \tilde{E}_\mathrm{z}} \tag{5}$$

where B_r, B_z, and B_t are the radial, vertical and toroidal magnetic field components, respectively. $A_1, \ldots, A_{10}$ are geometrical coefficients. $\tilde{E}_\mathrm{r}$ and $\tilde{E}_\mathrm{z}$ are proportional to the radial and vertical electric field components in the laboratory frame

$$\begin{aligned} \tilde{E}_\mathrm{r} &:= (E_\mathrm{r,dia} - v_\mathrm{tor} B_\mathrm{z})/v_\mathrm{beam} \; ; \; E_\mathrm{r,dia} := \frac{dp_\mathrm{I}/dr}{Z_\mathrm{I} e n_\mathrm{I}} \\ \tilde{E}_\mathrm{z} &:= (E_\mathrm{z,dia} + v_\mathrm{tor} B_\mathrm{r})/v_\mathrm{beam} \; ; \; E_\mathrm{z,dia} := \frac{dp_\mathrm{I}/dz}{Z_\mathrm{I} e n_\mathrm{I}} \end{aligned} \tag{6}$$

where $E_\mathrm{r,dia}$ and $E_\mathrm{z,dia}$ are the diamagnetic electric fields, v_tor the toroidal fluid rotation velocity (Fig. 4), p_I the pressure of impurity ion I, and v_beam the neutral beam velocity. On ASDEX Upgrade, a 93 keV deuterium beam is used for IMSE giving $v_\mathrm{beam} = 3.0 \times 10^6$ m/s. The poloidal fluid rotation in the plasma core can be neglected because the poloidal velocity at ASDEX Upgrade is typically far below 10^3 m/s[57]. The contribution of the poloidal rotation to the radial electric field is expected to be below 2 kV/m resulting in corrections of the absolute IMSE angles below 0.02° being significantly smaller than the resolution of the IMSE measurements. Note that for MSE measurements at the plasma edge the poloidal fluid rotation might become important due to the significant larger poloidal rotation velocity[58]. As will be depicted in section V.E, a reliable estimation of the electric fields is important

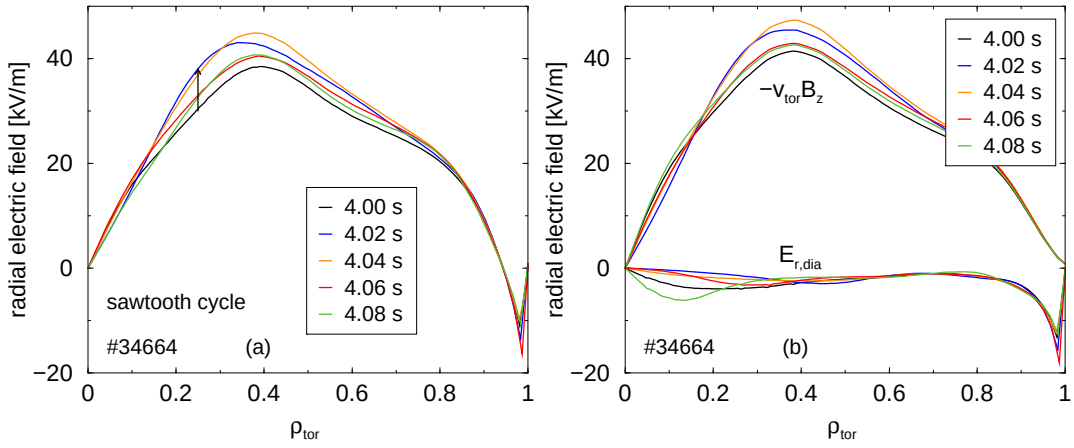

Fig. 11. Sawtooth cycle of (a) the radial electric field and (b) the diamagnetic and toroidal rotation components

for the interpretation of the MSE data. Fig. 11 shows an example sawtooth cycle of (a) the radial electric field profile and (b) the diamagnetic and toroidal rotation components. For the sawtooth cycle the large rotation component of the electric field is expected to be most important (see section V.E).

Although the absolute calibration of the IMSE is currently subject to ultimate fine-tuning, the sawtooth induced variation of the signal allows various modelling assumptions to be tested. Fig. 12 shows the measured IMSE angles (black circles) and the forward modelled

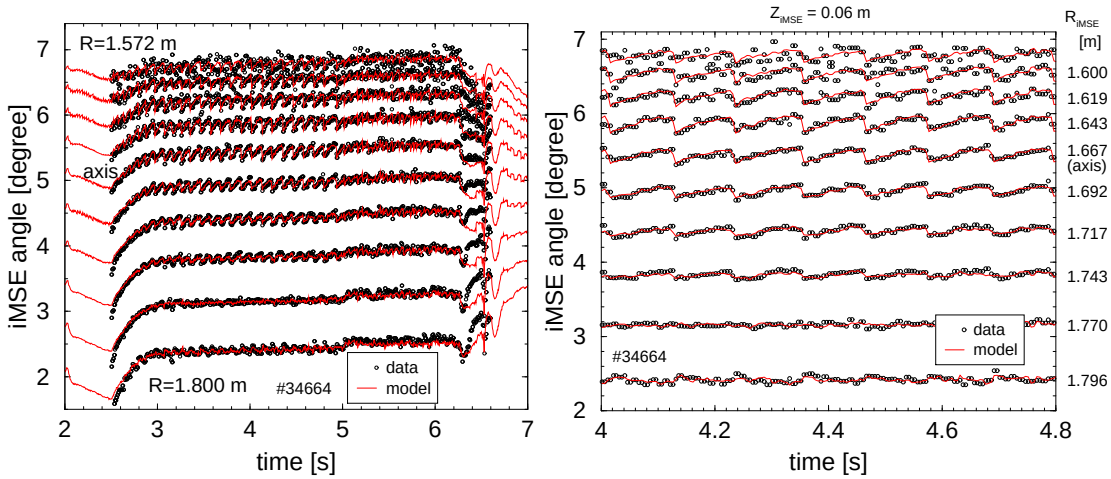

Fig. 12. Measured (black circles) and modelled (red line) IMSE data.

angles from the equilibrium (red line) using the FCM and fast-ion redistribution. 10 radial positions close to the midplane from $R = 1.57$–1.80 m are shown. The magnetic axis is at about $R_{\mathrm{mag}} = 1.66$–1.67 m (see Fig. 7). The statistical uncertainty of the IMSE angles is in the order of 0.05° only, although the absolute value is expected to have a somewhat larger

systematic uncertainty. The sawtooth induced jumps are up to 0.2° Although the IMSE data are not included in the set of data fitted by the equilibrium, the temporal evolution of the measured and modelled angles agrees very well. The absolute value of the angles are shifted to match the mean signal amplitude. On the high-field-side (hfs), $R < R_{\mathrm{mag}}$, the sawtooth events induce a decrease of the IMSE angles whereas on the far low-field-side (lfs) the behaviour is the opposite. Interestingly, the turning point is not at the magnetic axis but about 5 cm shifted to the lfs. This is the position where the effect of the inward shift of the magnetic axis and the effect of the sawtooth-induced current redistribution balance. The reduced Shafranov shift after the sawtooth event results in an inward shift of all plasma-core flux surfaces and, correspondingly, an increase (decrease) of the current measured at a particular IMSE channel at the lfs (hfs), respectively. The poloidal field and the corresponding IMSE angle increases or decreases, correspondingly. In contrast, the sawtooth-induced current redistribution reduces the current within the inversion radius, and, hence, reduces the poloidal field. On the hfs the two effects add up. In the very core the current redistribution dominates. At the outer lfs, $R > 1.77$ m, the effect of the Shafranov shift takes over since the total current within the respective flux surface is conserved.

The sawtooth induced changes in the modelled IMSE angles agree very well with the measured values if the redistribution of fast particles is considered. The agreement becomes worse if no redistribution is assumed. Fig. 13 shows a smaller region of Fig. 12 with modelled

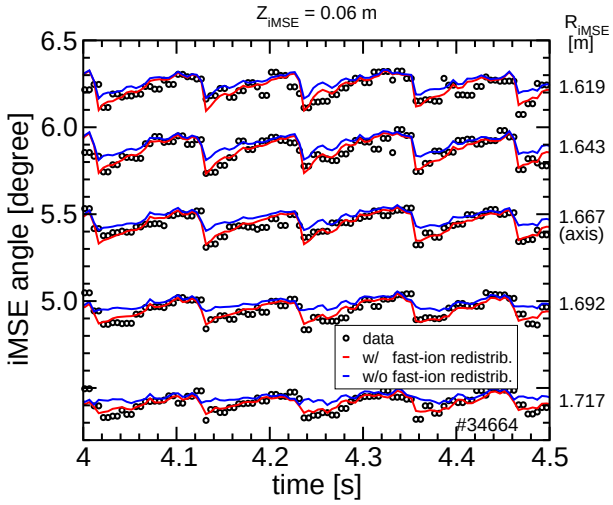

Fig. 13. IMSE angles measured (black circles) and modelled with (red line) and without (blue line) redistribution of fast-ions

IMSE angles assuming no fast-ion redistribution (blue line). Note that only the angle drop and recovery can be interpreted because the measured data are shifted to match the mean modelled angles assuming redistribution. The sawtooth induced change without fast-ion redistribution is significantly smaller and does no longer agree with the measured values. This can best be seen for IMSE channels close to the magnetic axis. Without redistribution the two opposing effects of the Shafranov shift and the current redistribution balance at about

2.5 cm from the axis to the lfs whereas the measured data clearly show that the effect by the current redistribution dominates. Obviously, for equilibrium estimation including the IMSE data a reliable quantification of the fast-ion redistribution is essential. Assuming no fast-ion redistribution the interpretation is complicated because additional to the reduced Shafranov shift also the equilibrium current and, hence, the sawtooth-induced current redistribution is changed. Fig. 14 shows the q-profiles with (red lines) and without (blue lines) fast-ion

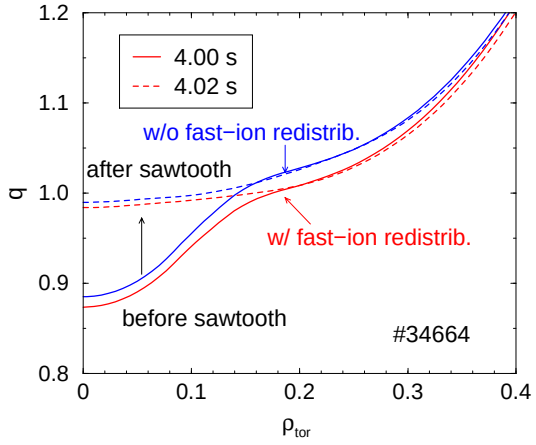

Fig. 14. q-profiles before (solid lines) and after (dashed lines) the sawtooth event comparing equilibria with (red) and without (blue) fast-ion redistribution.

redistribution before and after a sawtooth event at 4.013 s. The mixing radius as well as Δq change. Fig. 15 shows the evolution of q_0 with (red line) and without (blue line) fast-

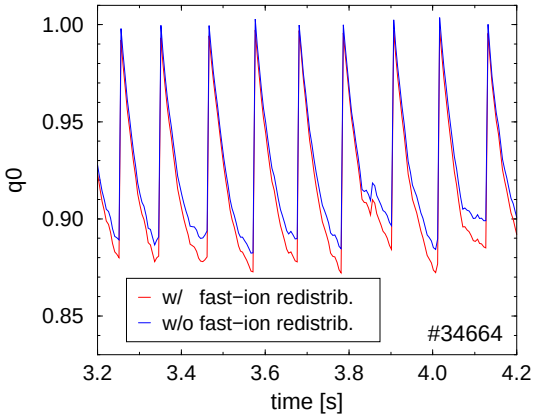

Fig. 15. Temporal evolution of q_0 with (red line) and without (blue line) fast-ion redistribution

ion redistribution. Although the different assumptions about the fast-ion redistribution result in apparently small changes in the q-profiles, the sawtooth induced Δq is comparable to the difference in q_0 between the Kadomtsev model and the FCM.

V.E. IMSE considering electric fields

Frequently, due to lack of suitable diagnostics, electric fields are not considered for the analysis of MSE measurements although its importance was described rather early[20,8]. Due to the small uncertainties of the IMSE angles already moderate electric fields are expected to have a large influence on their interpretation. Fig. 16 compares modelled MSE angles

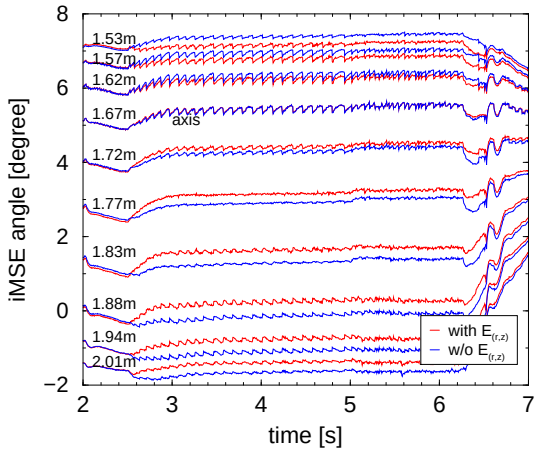

Fig. 16. Modelled IMSE angles with (red) and without (blue) electric fields

with (red line) and without (blue line) considering electric fields. At the magnetic axis the electric fields vanish leaving the angle unchanged. At off-axis positions there are rather large differences in absolute value ($\Delta\gamma \leq 0.4^\circ$) as well as smaller differences in the temporal behaviour due to sawtooth events.

The rotational term in equation (6) contributes most to the electric field in the plasma core (see Fig. 11). The diamagnetic term is of major importance only at the plasma edge. Note that at the plasma edge also the poloidal rotation has to be considered. The poloidal rotation is neglected for the present work as the IMSE measures in the plasma core only. Comparing the minor diamagnetic term (assuming $v_{\mathrm{tor}} = 0$) with the case without electric fields, a rather small shift of the MSE angles of $\Delta\gamma_{\mathrm{abs}} \leq 0.03^\circ$ and only a small reduction of the sawtooth-induced change $\Delta\gamma_{\mathrm{ST}} \leq 0.02^\circ$, depending on the location in the plasma, is observed. Considering the major rotational term only (assuming $E_{(\mathrm{r,z}),\mathrm{dia}} = 0$), the shift is much larger up to $\Delta\gamma_{\mathrm{abs}} = 0.4^\circ$. The change in the sawtooth-induced angle variation differs only by about $\Delta\gamma_{\mathrm{ST}} \leq 0.04^\circ$ comparing the two cases with and without the rotational term in the electric fields. Note that on the hfs the sawtooth-induced $\Delta\gamma_{\mathrm{ST}}$ is smaller considering the electric fields whereas on the lfs it is larger. Summarising, for a reliable interpretation of the IMSE measurements, the electric fields have to be considered. The sawtooth induced MSE angle change $\Delta\gamma_{\mathrm{ST}}$ is less affected by the electric fields, but, nevertheless, relevant for the estimation of the sawtooth Δq.

VI. Summary

The sawtooth induced q-profile evolution was modelled at ASDEX Upgrade and validated with IMSE measurements. The equilibrium current distribution was estimated coupling a Grad-Shafranov solver and the current diffusion equation. The extensive diagnostic suite at ASDEX Upgrade allows a reliable modelling of the current density profile and its temporal evolution as long as neo-classical current diffusion can be assumed. The diagnostics provide reliable kinetic electron and ion profiles, fast-ion density and pressure profiles, and rotation profiles with high temporal and spatial resolution. The equilibrium reconstruction is not constrained with internal current measurements. Nevertheless, the forward modelled MSE angles agree very well with the IMSE measurements.

The sawtooth-induced current relaxation is modelled with two different reconnection schemes, a Kadomtsev full reconnection model and a fully stochastic flat-current model (FCM). The Kadomtsev model results in an extended mixing zone with a current sheet at the mixing radius and $q_0 = 1$ after the reconnection whereas the FCM has a reduced mixing zone, $q_0 < 1$, and only a discontinuity in the current density at the mixing radius but no current sheet. Both models result in about the same sawtooth-induced $\Delta q_0 \approx 0.10$–0.12 but with slightly different absolute values. In contrast to the Kadomtsev model, the FCM conserves the position of the $q = 1$ flux surface and allows for a (1,1) sawtooth post-cursor mode at the $q = 1$ surface as seen in the experiment. For both models the helicity is nearly conserved slightly outside of the mixing radius.

The sawtooth-induced evolution of the modelled MSE angles agrees very well with the offset-corrected IMSE measurements. A sensitivity study reveals two major ingredients for a reliable interpretation of MSE measurements. Firstly, the sawtooth-induced redistribution of fast ions has to be taken into account for a reliable estimation of the Shafranov shift and the current distribution. A reliable estimation of the position of the flux surfaces relative to the position of the MSE channels is of major importance. The fast-ion redistribution is modelled with a particle-conserving homogeneous fast-ion pressure profile after the sawtooth event within $\rho_{\mathrm{tor}} \leq 0.6$ and a subsequent recovery time of 50 ms which represents experimental observations. A significant sawtooth-induced loss of fast particles can be excluded by simulating the diamagnetic flux with various loss schemes and comparing them with diamagnetic flux measurements. The results confirm previous experimental observations. Secondly, for the interpretation of the MSE angles a reliable estimation of the electric fields is required for both, the absolute value of the angles as well as for the sawtooth-induced changes.

ACKNOWLEDGEMENT

This work has been carried out within the framework of the EUROfusion Consortium and has received funding from the Euratom research and training programme 2014–2018 under grant agreement No 633053. The views and opinions expressed herein do not necessarily reflect those of the European Commission.

REFERENCES

References

[1] A. Bock, E. Fable, R. Fischer, M. Reich, D. Rittich, J. Stober, M. Bernert, A. Burckhart, H. Doerk, M. Dunne, B. Geiger, L. Giannone, V. Igochine, A. Kappatou, R. McDermott, A. Mlynek, T. Odstrčil, G. Tardini, H. Zohm, and the ASDEX Upgrade Team. Non-inductive improved H-mode operation at ASDEX Upgrade. *Nucl. Fusion*, 57:126041, 2017.

[2] A. Bock, H. Doerk, R. Fischer, D. Rittich, J. Stober, A. Burckhart, E. Fable, B. Geiger, A. Mlynek, M. Reich, H. Zohm, and the ASDEX Upgrade Team. Advanced tokamak investigations in full-tungsten ASDEX Upgrade. *Physics of Plasmas*, 25:056115, 2018.

[3] B. Nam, J.S. Ko, G.H. Choe, Y. Bae, M.J. Choi, W. Lee, G.S. Yun, S. Jardin, and H.K. Park. Validation of the 'full reconnection model' of the sawtooth instability in KSTAR. *Nucl. Fusion*, 58:066009, 2018.

[4] S. von Goeler, W. Stodiek, and N. Sauthoff. Studies of internal disruptions and m = 1 oscillations in tokamak discharges with soft–X-ray techniques. *Phys. Rev. Lett.*, 33:1201–1203, 1974.

[5] V. Igochine, editor. *Active Control of Magneto-hydrodynamic Instabilities in Hot Plasmas*. Springer, 2015.

[6] H. Soltwisch. Measurement of current-density changes during sawtooth activity in a tokamak by far-infrared polarimetry. *Rev. Sci. Instrum.*, 59:1599, 1988.

[7] F.M. Levinton. The multichannel motional Stark effect diagnostic on TFTR. *Rev. Sci. Instrum.*, 63:5157, 1992.

[8] B.W. Rice, D.G. Nilson, K.H. Burrell, and L.L. Lao. Simultaneous measurement of q and E_r profiles using the motional Stark effect in high-performance DIII-D plasmas. *Rev. Sci. Instrum.*, 70:815, 1999.

[9] J. Ko. Sensitivity of magnetic field-line pitch angle measurements to sawtooth events in tokamaks. *Rev. Sci. Instrum.*, 87:11E541, 2016.

[10] M.C.C. Messmer, J. Ko, , J. Chung, M.H. Woo, K.-D. Lee, and R.J.E. Jaspers. Evolution of the central safety factor during stabilized sawtooth instabilities at KSTAR. *Nucl. Fusion*, 58:016030, 2018.

[11] A. Burckhart, O. Ford, M. Reich, R. Wolf, and the ASDEX Upgrade Team. Design of the new Imaging Motional Stark Effect diagnostic at ASDEX Upgrade. In R. Bingham, Suttrop, S. Atzeni, R. Foest, K. McClements, B. Goncalves, C. Silva, and R. Coelho, editors, *EPS 2015 / Europhysics Conference Abstracts*, volume 39E, page P1.143. European Physical Society, Geneva, 2015.

[12] O. Ford, A. Burckhart, R. McDermott, T. Pütterich, R. C. Wolf, and ASDEX Upgrade Team. Imaging motional Stark effect measurements at ASDEX Upgrade. *Rev. Sci. Instrum.*, 87:11E537, 2016.

[13] A. Mlynek, R. Fischer, O. Ford, P. Lang, B. Plöckl, and ASDEX Upgrade Team. First results from the new sub-millimeter polarimeter on the ASDEX Upgrade tokamak. In *21st Topical Conference on High Temperature Plasma Diagnostics (HTPD 2016)*, 2016.

[14] H. Y. Yuh. *The Motional Stark Effect diagnostic on Alcator C-Mod*. PhD thesis, Massachusetts Institute of Technology, 2005.

[15] M. Reich, J. Hobirk, L.D. Horton, M. Maraschek, P.J. McCarthy, D. Merkl, and ASDEX Upgrade team. Calibration methods for the MSE diagnostic at ASDEX Upgrade. In *EPS 2007 / Europhysics Conference Abstracts*, volume 31F, page P2.127. European Physical Society, Geneva, 2007.

[16] M.A. Makowski, M. Brix, N.C. Hawkes, and the EFDA-JET Contributors. Semi-empirical calibration technique for the MSE diagnostic on the JET and DIII-D tokamaks. In *EPS 2008 / Europhysics Conference Abstracts*, volume 32D, page P4.085. European Physical Society, Geneva, 2008.

[17] H. Y. Yuh, F. M. Levinton, S. D. Scott, and J. Ko. Simulation of the motional Stark effect diagnostic gas-filled torus calibration. *Rev. Sci. Instrum.*, 79:10F523, 2008.

[18] C. T. Holcomb, M. A. Makowski, S. L. Allen, W. H. Meyer, and M. A. Van Zeeland. Overview of equilibrium reconstruction on DIII-D using new measurements from an expanded motional Stark effect diagnostic. *Rev. Sci. Instrum.*, 79:10F518, 2008.

[19] R. Fischer, A. Bock, M. Dunne, J.C. Fuchs, L. Giannone, K. Lackner, P.J. McCarthy, E. Poli, R. Preuss, M. Rampp, M. Schubert, J. Stober, W. Suttrop, G. Tardini, M. Weiland, and ASDEX Upgrade Team. Coupling of the flux diffusion equation with the equilibrium reconstruction at ASDEX Upgrade. *Fusion Sci. Technol.*, 69:526–536, 2016.

[20] B.W. Rice, D.G. Nilson, K.H. Burrell, and L.L. Lao. Effect of plasma radial electric field on motional stark effect measurements and equilibrium reconstruction. *Nucl. Fusion*, 37:517, 1997.

[21] R. Fischer, J. Hobirk, L. Barrera, A. Bock, A. Burckhart, I. Classen, M. Dunne, J.C. Fuchs, L. Giannone, K. Lackner, P.J. McCarthy, E. Poli, R. Preuss, M. Rampp, S.K. Rathgeber, M. Reich, B. Sieglin, W. Suttrop, E. Wolfrum, and ASDEX Upgrade Team. Magnetic equilibrium reconstruction using geometric information from temperature measurements at ASDEX Upgrade. In V. Naulin, C. Angioni, and M. Borghesi et al., editors, *40th EPS Conference on Plasma Physics*, volume 37D, page P2.139. European Physical Society, Geneva, 2013.

[22] G. Pereverzev and P.N. Yushmanov. ASTRA automated system for transport analysis in a tokamak. Technical Report IPP 5/98, Max-Planck-Institut für Plasmaphysik, Garching, 2002.

[23] M. Weiland, R. Bilato, R. Dux, B. Geiger, A. Lebschy, F. Felici, R. Fischer, D. Rittich, M. Van Zeeland, the ASDEX Upgrade team, and the Eurofusion MST1 team. RABBIT: Real-time simulation of the NBI fast-ion distribution. *Nucl. Fusion*, 58:082032, 2018.

[24] R. Fischer, C.J. Fuchs, B. Kurzan, W. Suttrop, E. Wolfrum, and ASDEX Upgrade Team. Integrated data analysis of profile diagnostics at ASDEX Upgrade. *Fusion Sci. Technol.*, 58:675–684, 2010.

[25] R. M. McDermott, A. Lebschy, B. Geiger, C. Bruhn, M. Cavedon, M. Dunne, R. Dux, R. Fischer, A. Kappatou, T. Pütterich, E. Viezzer, and ASDEX Upgrade Team. Extensions to the charge exchange recombination spectroscopy diagnostic suite at ASDEX Upgrade. *Rev. Sci. Instrum.*, 88:073508, 2017.

[26] R. M. McDermott, C. Angioni, G.D. Conway, R. Dux, E. Fable, R. Fischer, T. Pütterich, F. Ryter, E. Viezzer, and the ASDEX Upgrade Team. Core intrinsic rotation behaviour in ASDEX Upgrade ohmic L-mode plasmas. *Nucl. Fusion*, 54:043009, 2014.

[27] S.K. Rathgeber, R. Fischer, S. Fietz, J. Hobirk, A. Kallenbach, H. Meister, T. Pütterich, F. Ryter, G. Tardini, E.Wolfrum, and the ASDEX Upgrade Team. Estimation of profiles of the effective ion charge at ASDEX Upgrade with Integrated Data Analysis. *Plasma Phys. Control. Fusion*, 52:095008, 2010.

[28] L. Giannone, R. Fischer, J.C. Fuchs, B. Geiger, M. Maraschek, D. Rittich, B. Sieglin, A. Bock, J. Hobirk, A. Kallenbach, V. Mertens, K.H. Schuhbeck, , and P.J. McCarthy. Note: Internal diamagnetic flux measurements on ASDEX Upgrade. *Rev. Sci. Instrum.*, 89:106101, 2018.

[29] B. B. Kadomtsev. Disruptive instability in tokamaks. *Sov. J. Plasma Phys.*, 1:389–391, 1975.

[30] F. Porcelli, D. Boucher, and M.N. Rosenbluth. Model for the sawtooth period and amplitude. *Plasma Phys. Control. Fusion*, 38:2163–2186, 1996.

[31] V. Igochine, O. Dumbrajs, H. Zohm, A. Flaws, and the ASDEX Upgrade Team. Stochastic sawtooth reconnection in ASDEX Upgrade. *Nucl. Fusion*, 47:23–32, 2007.

[32] O. Dumbrajs, V. Igochine, H. Zohm, and the ASDEX Upgrade Team. Diffusion in a stochastic magnetic field in ASDEX Upgrade. *Nucl. Fusion*, 48:024011, 2008.

[33] M-C. Firpo, A. F. Lifschitz, W. Ettoumi, R. Farengo, H. E. Ferrari, and P. L. García-Martínez. Evidence and relevance of spatially chaotic magnetic field lines in MCF devices. *Plasma Phys. Control. Fusion*, 59:034005, 2017.

[34] J.A.Wesson. Sawtooth oscillations. *Plasma Phys. Control. Fusion*, 28:243, 1986.

[35] Ya.I. Kolesnichenko, Yu.V. Yakovenko, D. Anderson, M. Lisak, and F. Wising. Sawtooth oscillations with the central safety factor, q_0, below unity. *Phys. Rev. Lett.*, 68:3881, 1992.

[36] A. Gude, M. Maraschek, O. Kardaun, and the ASDEX Upgrade team. An automated sawtooth detection algorithm for strongly varying plasma conditions and crash characteristics. *Plasma Phys. Control. Fusion*, 59:095009, 2017.

[37] E. Priest and T. Forbes. *Magnetic Reconnection: MHD Theory and Applications*. Cambridge University Press, New York, 2000. Chapter 4.

[38] J. Wesson. *Tokamaks*. Oxford University Press, 2011. Chapter 7.

[39] Ya.I. Kolesnichenko and Yu.V. Yakovenko. Theory of fast ion transport during sawtooth crashes in tokamaks. *Nucl. Fusion*, 36:159, 1996.

[40] V. Igochine, J. Boom, I. Classen, O. Dumbrajs, S. Günter, K. Lackner, G. Pereverzev, H. Zohm, and the ASDEX Upgrade Team. Structure and dynamics of sawteeth crashes in ASDEX Upgrade. *Phys. Plasmas*, 17:122506, 2010.

[41] D. Vezinet, V. Igochine, M. Weiland, Q. Yu, A. Gude, D. Meshcheriakov, M. Sertoli, the ASDEX Upgrade Team, and the EUROfusion MST1 Team. Non-monotonic growth rates of sawtooth precursors evidenced with a new method on ASDEX Upgrade. *Nucl. Fusion*, 56:086001, 2016.

[42] G. Bateman, C. N. Nguyen, A. H. Kritz, and F. Porcelli. Testing a model for triggering sawtooth oscillations in tokamaks. *Physics of Plasmas*, 13:072505, 2006.

[43] V. Igochine, O. Dumbrajs, and H. Zohm the ASDEX Upgrade Team. Transition from quasiperiodicity to chaos just before sawtooth crash in the ASDEX Upgrade tokamak. *Nucl. Fusion*, 48:062001, 2008.

[44] J.B. Taylor and S.L. Newton. Lecture notes: Special topics in plasma confinement. *J. Plasma Phys.*, 81:205810501, 2015.

[45] M.A. Berger. Introduction to magnetic helicity. *Plasma Phys. Control. Fusion*, 41:B167–B175, 1999.

[46] D.D. Schnack. *Lectures in Magnetohydrodynamics*. Springer, 2009.

[47] A. Bhattacharjee and R.L. Dewar. Energy principle with global invariants. *Phys. Fluids*, 25:887, 1982.

[48] W.W. Heidbrink and T.H. Dang. Magnetic helicity is conserved at a tokamak sawtooth crash. *Plasma Phys. Control. Fusion*, 42:L31–L36, 2000.

[49] S. S. Denk, R. Fischer, H. M. Smith, P. Helander, O. Maj, E. Poli, J. Stober, U. Stroth, W. Suttrop, E. Westerhof, M. Willensdorfer, and the ASDEX Upgrade Team. Analysis of electron cyclotron emission with extended electron cyclotron forward modeling. *Plasma Phys. Control. Fusion*, 60:105010, 2018.

[50] B. Kurzan and H. D. Murmann. Edge and core Thomson scattering systems and their calibration on the ASDEX Upgrade tokamak. *Rev. Sci. Instrum.*, 82:103501, 2011.

[51] M. Willensdorfer, G. Birkenmeier, R. Fischer, F. M. Laggner, E. Wolfrum, G. Veres, F. Aumayr, D. Carralero, L. Guimarãis, B. Kurzan, and the ASDEX Upgrade Team. Characterization of the Li-BES at ASDEX Upgrade. *Plasma Phys. Control. Fusion*, 56:025008, 2014.

[52] B. Geiger, M. Garcia-Munoz, R. Dux, F. Ryter, G. Tardini, L. Barrera Orte, I.G.J. Classen, E. Fable, R. Fischer, V. Igochine, R.M. McDermott, and the ASDEX Upgrade Team. Fast-ion transport in the presence of magnetic reconnection induced by sawtooth oscillations in ASDEX Upgrade. *Nucl. Fusion*, 54:022005, 2014.

[53] B. Geiger, M. Weiland, A. Mlynek, M. Reich, A. Bock, M. Dunne, R. Dux, E. Fable, R. Fischer, M. Garcia-Munoz, J. Hobirk, C. Hopf, S. Nielsen, T. Odstrčil, C. Rapson,

D. Rittich, F. Ryter, M. Salewski, P. A. Schneider, G. Tardini, M. Willensdorfer, and the ASDEX Upgrade Team. Quantification of the impact of large and small-scale instabilities on the fast-ion confinement in ASDEX Upgrade. *Plasma Phys. Control. Fusion*, 57:014018, 2015.

[54] M. Weiland, B. Geiger, A. S. Jacobsen, M. Reich, M. Salewski, T. Odstrčil, and the ASDEX Upgrade Team. Enhancement of the FIDA diagnostic at ASDEX Upgrade for velocity space tomography. *Plasma Phys. Control. Fusion*, 58:025012, 2016.

[55] Z.A. Pietrzyk, A. Pochelon, T.P. Goodman, M.A. Henderson, J.-P. Hogge, H. Reimerdes, M.Q. Tran, R. Behn, I. Furno, J.-M. Moret, C. Nieswand, J. Rommers, O. Sauter, W. van Toledo, H. Weisen, F. Porcelli, and K.A. Razumova. Behaviour of central plasma relaxation oscillations during localized electron cyclotron heating on the TCV tokamak. *Nucl. Fusion*, 39:587, 1999.

[56] A. Gude. Identification of MHD instabilities in experiments. In V. Igochine, editor, *Active Control of Magneto-hydrodynamic Instabilities in Hot Plasmas*, pages 53–104. Springer, 2015. Chapter 3.

[57] A. Lebschy, R.M. McDermott, C. Angioni, B. Geiger, D. Prisiazhniuk, M. Cavedon, G.D. Conway, R. Dux, M.G. Dunne, A. Kappatou, T. Pütterich, U. Stroth, , E. Viezzer, and the ASDEX Upgrade Team. Measurement of the complete core plasma flow across the LOC–SOC transition at ASDEX Upgrade. *Nucl. Fusion*, 58:026013, 2018.

[58] E. Viezzer, T. Pütterich, G.D. Conway, R. Dux, T. Happel, J.C. Fuchs, R. M. McDermott, F. Ryter, B. Sieglin, W. Suttrop, M. Willensdorfer, E. Wolfrum, and the ASDEX Upgrade Team. High-accuracy characterization of the edge radial electric field at ASDEX Upgrade. *Nucl. Fusion*, 53:053005, 2013.